Modeling, Identification, and Optimal Control of Batteries for Power System Applications

Philipp Fortenbacher
ETH Zurich, Switzerland
fortenbacher@eeh.ee.ethz.ch

Johanna L. Mathieu
University of Michigan, USA
jlmath@umich.edu

Göran Andersson
ETH Zurich, Switzerland
andersson@eeh.ee.ethz.ch

***Abstract*—This paper proposes a novel algorithm to identify degradation in batteries used for power system applications. Unlike conventional battery control methods that try to extend battery lifetime by applying heuristic rules, this approach allows us to maximize battery lifetime within an optimal control framework. We use an online Least Squares (LS) identification method to develop a two-dimensional degradation map that describes the lost battery charge as a function of the battery state of charge and the applied current. We project the degradation map to an economic cost function that associates each discrete control action with its utilization cost. Additionally, we develop a nonlinear battery model to capture fast battery dynamics including the rate capacity effect and we identify its parameters with a nonlinear LS method. We demonstrate the usefulness of the approach by presenting a model predictive control (MPC) scheme for a peak shave application in which we use a linearized version of the battery model along with the degradation cost function. We use a high-fidelity lithium ion electrochemical battery model to simulate a real battery system and we show that the MPC scheme increases the battery lifetime by a factor of 2.6 and the internal rate of return by 11 percentage points as compared to conventional control approaches.**

***Keywords*—battery modeling, capacity fade, battery degradation, online system identification, battery management systems, battery energy storage system**

I. Introduction

Investment costs for batteries used in power system applications are still very high [1], such that a battery's expected lifetime greatly affects assessments of its economic viability. Battery investment decisions usually rely on utilization costs derived from integral terms such as the total number of achievable cycles by a pre-defined end of life capacity [2]. However, in reality, there is a nonlinear relationship between operational management and charge capacity loss, and so the total amount of energy that can be delivered in a battery's lifetime is dependent on each individual control action. Thus, operational management has a strong influence on profitability and we can best address economic requirements by developing control policies that take battery lifetime into account.

Instead of using heuristic rules to minimize battery degradation [3], one can use a Model Predictive Control (MPC) framework to obtain near-optimal results. Since MPC relies on dynamic models and control objectives, we need quantitative models of both the slow battery degradation process and the fast dynamics. A common approach used to quantify degradation involves using available manufacturer data that specify capacity loss under constant cycling [4]. However, these data do not allow us to accurately determine an individual battery's capacity loss under other types of cycling, such as those required for power system applications.

The contribution of this paper is the development of methods to identify both fast battery dynamics and slow battery degradation processes given arbitrary battery usage patterns. The models are identified with data from a high-fidelity electrochemical lithium ion (Li-ion) battery model [5] used in place of a real battery system. We present a linearized model of the fast battery dynamics, which allows us to use a linear optimization framework. Importantly, the model captures the rate capacity effect [6] allowing us to accurately model the capabilities of the battery in high/low state of charge (SOC) regimes. Furthermore, we introduce an online Identification (ID) method that maps the lost charge capacity associated with each discrete control action to the SOC and current, allowing us to create a battery degradation map. Additionally, we propose an economically-motivated quadratic control objective derived from the degradation map and show how it can be incorporated into an MPC framework, which includes the fast battery dynamics. Through an example, we show how this strategy increases both the battery lifetime and the Internal Rate of Return (IRR) compared to conventional control methods, e.g., [7], [8]. The paper includes the following parts. Section II describes the battery models, system identification methods, and model validation results. Section III presents the derivation of a quadratic cost function that relates battery degradation and utilization costs. Section IV describes a typical power system application and compares the results of the MPC approach to those of several conventional approaches. Section V concludes and provides an outlook for future research.

II. Battery Modeling and System Identification

We propose a two-stage ID process consisting of 1) parameter estimation of models that capture the fast battery dynamics and 2) identification of the slow battery degradation process, which we refer to as 'capacity fade.' First, we introduce several different battery models and estimate their parameters from data obtained from the electrochemical battery model DUALFOIL [5]. Second, we identify the capacity fade, again using data from the DUALFOIL model. We assume a stationary degradation process.

A. Fast Dynamics

Ref. [9] presented a nonlinear battery model consisting of one internal resistor R, the value of which depends mainly on the ion conductivity of the electrolyte. The accessible electric charge $Q_{\rm bat}$ is limited by the cut-off voltages of the cell, and the SOC keeps track of the level of the remaining charge normalized by $Q_{\rm bat}$. We refer to this as the *nonlinear basic battery model*

$$\dot{\rm SOC} = -{Q_{\rm bat}}^{-1} I_{\rm bat} \quad , \tag{1}$$
$$V_{\rm t} = f_{\rm ocv}({\rm SOC}) - R I_{\rm bat} \quad , \tag{2}$$

where $V_{\rm t}$ is the terminal output voltage and $I_{\rm bat}$ is the input current. Unlike [9], we assume the nonlinear open circuit voltage function $f_{\rm ocv}$ is known via a lookup table.

This model does not capture the dependency of the battery capacity on the charge rate, referred to as the 'rate capacity effect' [6]. To capture this behavior, we extend (1)-(2) using dynamics from the KiBaM model [10], which includes two charge capacity wells (x_1, x_2). Charge can be withdrawn only from the available well x_1 and the wells are connected internally with a valve. The dimensionless parameters $c_{\rm r}$ and $c_{\rm w}$ define the conductance of the valve and the width of the available charge well, respectively. The KiBAM model describes only lead acid batteries, and so we have modified the system output equation to include $f_{\rm ocv}$ to represent different battery technologies such as Li-ion and NaS. Therefore, our *nonlinear extended battery model* is

$$\underbrace{\begin{bmatrix} \dot{x_1} \\ \dot{x_2} \end{bmatrix}}_{\dot{\boldsymbol{x}}} = \underbrace{\begin{bmatrix} -\frac{c_{\rm r}}{c_{\rm w}} & \frac{c_{\rm r}}{1-c_{\rm w}} \\ \frac{c_{\rm r}}{c_{\rm w}} & -\frac{c_{\rm r}}{1-c_{\rm w}} \end{bmatrix}}_{\boldsymbol{A}} \boldsymbol{x} - \begin{bmatrix} Q_{\rm bat}^{-1} \\ 0 \end{bmatrix} I_{\rm bat} \, , \tag{3}$$
$$V_{\rm t} = f_{\rm ocv}\left(\frac{x_1}{c_{\rm w}}\right) - R I_{\rm bat} \quad , \tag{4}$$

where ${\rm SOC} = x_1 + x_2$. Note that we normalize the charge wells by the charge capacity $Q_{\rm bat}$, which is an additional difference between this model and the KiBaM model.

We can linearize the battery models by setting $f_{\rm ocv}(\cdot)$ to a constant value $\bar{V}_{\rm oc}$. If we neglect the power converter dynamics, we can multiply the output equations (2) and (4) by the battery current $I_{\rm bat}$ to obtain an expression for the battery power

$$P_{\rm bat} = V_{\rm t} I_{\rm bat} = \bar{V}_{\rm oc} I_{\rm bat} - R {I_{\rm bat}}^2 \quad . \tag{5}$$

We can also obtain a version of (1)-(2) that is linear in power. We first solve (5) for $I_{\rm bat}$. Figure 1 shows the region around the real root of $I_{\rm bat}$. We linearly approximate the charging and discharging current up to the battery's rated power $P_{\rm bat,r}$, as shown in the figure. We then insert the linearized currents into

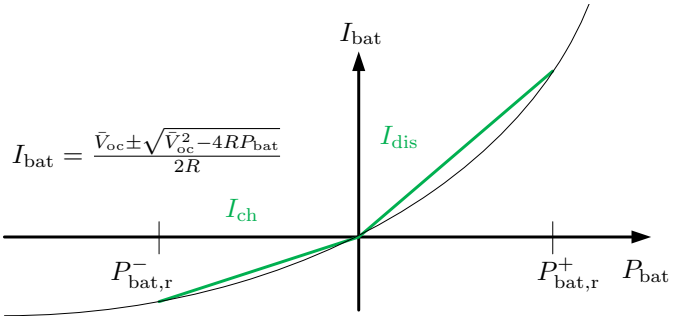

Figure 1. Linearization of the charging $I_{\rm ch}$ and discharging $I_{\rm dis}$ currents, given rated power $P_{\rm bat,r}$.

(1)-(2) and multiply (1) by $\bar{V}_{\rm oc}$. With following definitions

$$C_{\rm bat} = Q_{\rm bat} \bar{V}_{\rm oc} \quad , \tag{6}$$
$${\eta_{\rm gen}}^{-1} = \frac{\bar{V}_{\rm oc} - \sqrt{\bar{V}_{\rm oc}^2 - 4RP^+_{\rm bat,r}}}{2RP^+_{\rm bat,r}} \bar{V}_{\rm oc} \quad , \tag{7}$$
$$\eta_{\rm load} = \frac{\bar{V}_{\rm oc} - \sqrt{\bar{V}_{\rm oc}^2 - 4RP^-_{\rm bat,r}}}{-2RP^-_{\rm bat,r}} \bar{V}_{\rm oc} \quad , \tag{8}$$
$$u^{\rm bat}_{\rm load} = \begin{cases} -P_{\rm bat} & \text{if } P_{\rm bat} < 0 \\ 0 & \text{if } P_{\rm bat} \geq 0 \end{cases} \, , \tag{9}$$
$$u^{\rm bat}_{\rm gen} = \begin{cases} P_{\rm bat} & \text{if } P_{\rm bat} > 0 \\ 0 & \text{if } P_{\rm bat} \leq 0 \end{cases} \, , \tag{10}$$

we obtain the following *linear basic battery model*

$$\dot{x} C_{\rm bat} = -{\eta_{\rm gen}}^{-1} u^{\rm bat}_{\rm gen} + \eta_{\rm load} u^{\rm bat}_{\rm load} \quad , \tag{11}$$
$$V_{\rm t} = \bar{V}_{\rm oc} - \frac{R}{\bar{V}_{\rm oc}} (u^{\rm bat}_{\rm gen} - u^{\rm bat}_{\rm load}) \quad , \tag{12}$$

where (11) is a Power Node equation [11] with efficiency parameters $\eta_{\rm gen}$ and $\eta_{\rm load}$, energy capacity $C_{\rm bat}$, power extraction/injection variables $u_{\rm gen}$ and $u_{\rm load}$, and $x = {\rm SOC}$. The linearized model can be extended to include the rate capacity effect from (3) yielding the *linear extended battery model*

$$\dot{\boldsymbol{x}} = \boldsymbol{A}\boldsymbol{x} + {C_{\rm bat}}^{-1} \begin{bmatrix} -\eta_{\rm gen}^{-1} & \eta_{\rm load} \\ 0 & 0 \end{bmatrix} \begin{bmatrix} u_{\rm gen} \\ u_{\rm load} \end{bmatrix} , \tag{13}$$
$$V_{\rm t} = \bar{V}_{\rm oc} - \frac{R}{\bar{V}_{\rm oc}} (u_{\rm gen} - u_{\rm load}) \quad . \tag{14}$$

The battery models are identified and validated on the DUALFOIL model configured, as shown in Table I, to include stationary chemical side reactions that cause irreversible battery capacity loss. The DUALFOIL model is a highly accurate battery model that captures the electrochemical process with partial differential algebraic equations solved with a Newton-Raphson variable step solver. For our economic assessment, we use an end of life (eoL) criterion that defines the proportion of battery capacity remaining at the end of the battery's useful life. Specifically, to get degradation results comparable to a standard cycling test, we tune the parameters $r_{\rm sc}$ and $r_{\rm sa}$ such that after 4000 full cycles the initial charge capacity is reduced

Table I
DUALFOIL CONFIGURATION

ambient conditions	isothermal	
cathode	$LiCoO_2$	
anode	Graphite	
electrolyte	$LiPF_6$	
A_{cell}	1 m^2	cell area
r_{sc}	1e-11	side reaction rate constant cathode
r_{sa}	1e-11	side reaction rate constant anode

Table II
IDENTIFIED PARAMETERS OF PROPOSED BATTERY MODELS BASED ON DATA FROM THE DUALFOIL MODEL

R	1.5 mΩ	internal resistance
Q_{bat}	31.25 Ah	charge capacity
c_{w}	0.93	charge well factor
c_{r}	2.24e-5	recovery factor
η_{load}	0.98	charge efficiency
η_{gen}	0.97	discharge efficiency
C_{bat}	120 Wh	energy capacity

by approximately 20% (i.e. eoL = 0.8). We calculate the 'true' values of the SOC and capacity fade from the internal DUALFOIL electrode utilization variables and use them for model ID and validation. We identify the parameters of the nonlinear battery models and then use them to compute the linear battery model parameters with (6)-(8). To identify the parameters, we use a Nonlinear Least Squares (NLS) approach

$$\hat{\boldsymbol{\theta}} = \arg\min_{\boldsymbol{\theta}} \sum_{k=1}^{N} (V_{\text{t,meas}}(k) - V_{\text{t,model}}(I_{\text{bat}}(k), \boldsymbol{\theta}, \boldsymbol{x}_0))^2 \quad , \tag{15}$$

where the nonlinear basic battery model parameter vector $\boldsymbol{\theta}_b^T = [R \quad Q_{\text{bat}}]^T$, nonlinear extended battery model parameter vector $\boldsymbol{\theta}_e^T = [R \quad Q_{\text{bat}} \quad c_{\text{w}} \quad c_{\text{r}}]^T$, and $\boldsymbol{x}_0$ is the initial state vector. We use a Constant Current - Constant Voltage (CC-CV) charging/recharging pattern as an input stimuli (Fig. 2, lower panel), start with a fully depleted battery so $\boldsymbol{x}_0 = \mathbf{0}$, and assume perfect state measurements, which means that we know the SOC of the nonlinear models perfectly. The identified parameters are listed in Table II. After identifying the nonlinear battery models, we plot their outputs for the same input sequence used during ID, shown in Fig. 2, upper panel. The output of the nonlinear extended battery model matches that of the DUALFOIL model well since it captures the rate capacity effect. During the CV phases, the output of the nonlinear basic battery model cannot closely follow that of the DUALFOIL model. To compare the performance of all four models in terms of their state and output prediction errors, we use the Normalized Root Mean Squared Error (NRMSE) defined as

$$\text{NRMSE} = \frac{\|\boldsymbol{y}_m - \boldsymbol{y}\|_2}{\|\boldsymbol{y} - \bar{y}\|_2} \quad , \tag{16}$$

where $\boldsymbol{y}_m$ is the state/output prediction, $\boldsymbol{y}$ is the state/output of the 'true system' (DUALFOIL model), and $\bar{y}$ is the mean value of $\boldsymbol{y}$. The results are summarized in Table III. The SOC predictions from the linearized models match very well with that of the DUALFOIL model. Therefore, it can be concluded that the current and open circuit voltage linearization do not have a significant impact on the state prediction error.

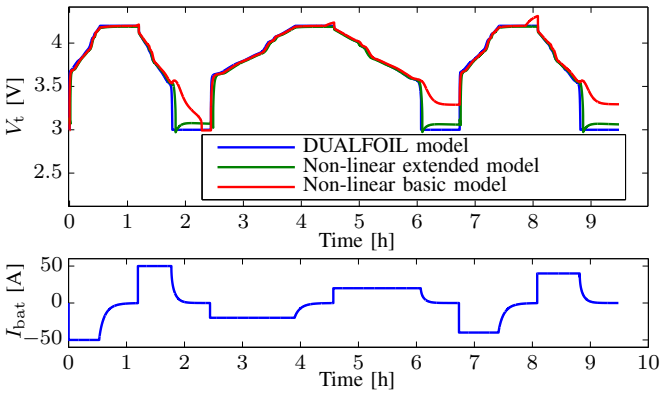

Figure 2. Model validation of the nonlinear battery models against the DUALFOIL model.

Table III
SUMMARY OF MODEL NRMSES

Model	SOC error [%]	V_t error [%]
nonlinear basic	0	38
nonlinear extended	0	18
linear basic	3	98
linear extended	3	59

However, the linearizations result in high output prediction error for both linear models. We use the linear extended battery model within our MPC controller. We also use this model together with a Luenberger observer to estimate the model states (x_1, x_2) using SOC measurements from the DUALFOIL model. The model state estimates are needed within the controller.

B. Slow Dynamics

Battery degradation depends on battery operation and can thus be influenced by the operational management. Degradation processes are very hard to model, and even in the electrochemical domain there does not exist a complete theory [12]. Among the contributors to capacity fade are two chemical side reactions that transform cyclable ions into solids during battery operation. Solid deposition occurs on both the cathode and anode at charging and discharging. While on the cathode side the electrolyte dissociates into solid particles, a thin film is deposited on the anode, leading to an increase in the internal resistance [12].

Side reactions are activated by 1) potential differences between the interfaces of electrolyte and electrodes, 2) temperature, and 3) the applied battery current [12]. The reaction rate, defined as the number of ions converted into solid materials per time, is related to the side current

$$I_{\text{s}} = -\dot{Q}_{\text{bat}} = f(V_{\text{oc}}, I_{\text{bat}}, \vartheta) \quad , \tag{17}$$

where ϑ is the temperature. Since this process takes place internally, this current cannot be measured directly. Also, measurement of the internal resistance is not sufficient for determining the complete degradation process because it is affected by only the anode layer decomposition. The lost

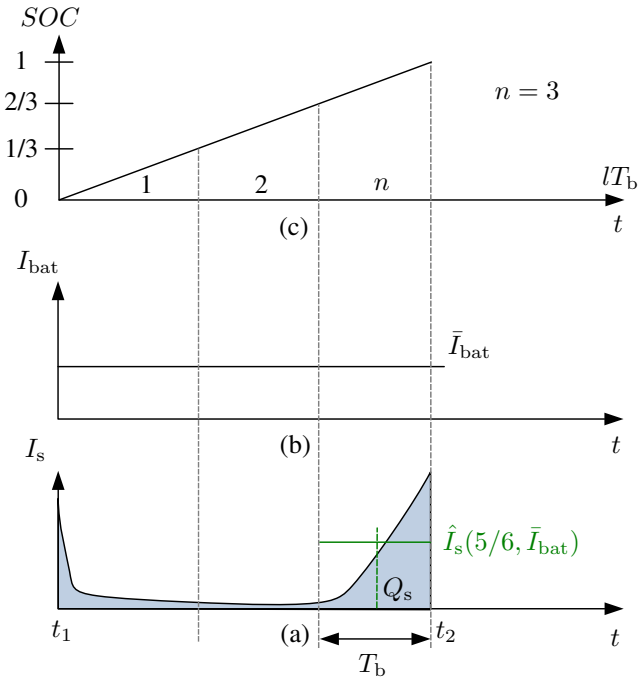

Figure 3. Illustration of the side current (a) given a constant applied battery current I_{bat} (b), which results in a linearly increasing SOC (c). In (a), the blue area shows the actual lost charge Q_{s}, while the green line shows the approximated value within SOC band $n = 3$.

charge can only be measured over long observation periods [13]. Hence, it cannot be directly associated with individual control actions. However, if there are many charge capacity measurements, it is possible to estimate the charge lost from discrete types of control actions. We characterize a control action by the applied battery current and the battery's SOC, and so we discretize these two values into n SOC 'bands' and m current 'intervals.' We then assume that the side current is a function of these values (note that we assume isothermal battery operation so we neglect the direct effect of temperature).

Figure 3 shows an example. The lost charge Q_s between time t_1 and time t_2 is

$$Q_{\text{s}} = Q_{\text{bat}}(t_1) - Q_{\text{bat}}(t_2) = \int_{t_1}^{t_2} I_{\text{s}}(\text{SOC}(t), I_{\text{bat}}(t))\text{d}t\,, \quad (18)$$

which is shown in blue in Fig. 3(a). In this example, we discretize the SOC range into $n = 3$ SOC bands (Fig. 3(c)) so that we can divide Q_s into discretized side current values, each associated with an SOC band and current interval. Then, Q_s can be approximated as the sum of the discretized side current values

$$Q_{\text{s}} \approx \sum_{l=1}^{n} \hat{I}_{\text{s}}\left(\text{SOC}(l), \bar{I}_{\text{bat}}\right) T_{\text{b}} \quad , \quad (19)$$

where $\bar{I}_{\text{bat}}$ is the current associated with the relevant current interval and T_{b} is the time it takes the SOC to traverse the SOC band given $\bar{I}_{\text{bat}}$. The relevant current interval is determined by calculating the mean current applied to the battery when it was within the SOC band associated with center $\left(\frac{2l-1}{2n}\right)$. Note that both T_{b} and $\bar{I}_{\text{bat}}$ are constant in this example, but are not in the general case.

For multiple capacity loss measurements $(Q_{\text{s},1}, ..., Q_{\text{s},i})$ and arbitrary stimuli patterns, the unknown discretized side current values can be arranged into a system of linear equations

$$\underbrace{\begin{bmatrix} \sum_{j=1}^{m}\sum_{l=1}^{n} p_{1,(n(j-1)+l)}\, T_{\text{b},j}\, \hat{I}_{\text{s}}\left(\frac{2l-1}{2n}, \bar{I}_{\text{bat},j}\right) \\ \vdots \\ \sum_{j=1}^{m}\sum_{l=1}^{n} p_{i,(n(j-1)+l)}\, T_{\text{b},j}\, \hat{I}_{\text{s}}\left(\frac{2l-1}{2n}, \bar{I}_{\text{bat},j}\right) \end{bmatrix}}_{\boldsymbol{M}\hat{\boldsymbol{I}}_{\text{s}}} = \underbrace{\begin{bmatrix} Q_{\text{s},1} \\ \vdots \\ Q_{\text{s},i} \end{bmatrix}}_{\boldsymbol{Q}_{\text{s}}} \quad , \quad (20)$$

where the p counts the control actions associated with each SOC band and current interval. We estimate $\boldsymbol{I}_{\text{s}}$ with Least Squares (LS)

$$\begin{aligned} \hat{\boldsymbol{I}}_{\text{s}} &= \arg\min_{\hat{\boldsymbol{I}}_{\text{s}}} \|\boldsymbol{M}\hat{\boldsymbol{I}}_{\text{s}} - \boldsymbol{Q}_{\text{s}}\|_2^2 \quad , \\ &\text{s.t.} \quad \hat{\boldsymbol{I}}_{\text{s}} > 0 \quad . \end{aligned} \quad (21)$$

We apply the degradation ID method to the DUALFOIL model forced with a random current pattern. We discretize the SOC range into 10 SOC bands and the applied battery current into 3 current intervals. This means that at least 30 measurements of Q_{bat} are needed to obtain a unique solution for the side currents. We identify the system after 180 approximately full cycles, which constitutes approximately 5% of the battery lifetime. Hence, we measure Q_{bat} every 6 approximately full cycles. Figure 4 shows the SOC variation and battery degradation during the ID process. We also plot the degradation model output prediction (green line) for the same current pattern. The low Root Mean Squared Error (RMSE) tells us that using 30 discrete types of control actions is sufficient for reproducing the lost charge values from the DUALFOIL model. Figure 5 shows how I_{s} varies as a function of the SOC and applied battery current. We plot values obtained from the DUALFOIL model along with a 'degradation map' derived through ID. Capacity fade increases exponentially at high SOCs and high currents. This is in line with theory since the anode side reaction takes place at high potentials corresponding to high SOCs. Degradation is also high at low SOCs because of the cathode side reaction. The models match well; however, we observe some differences at low SOCs because our discretization results in smoothing.

III. Economic Battery Cost Function

To operate a battery in an economically-efficient way, we need to quantify the economic utilization costs, which include the operating costs (for example, resulting from losses and degradation) and the investment costs per total delivered energy c_{inv} subject to the eoL criterion.

To calculate the costs associated with degradation, we can apply the following transformation

$$\frac{\text{Costs}}{C_{\text{bat}}} = \frac{I_{\text{s}} c_{\text{inv}}}{(1 - \text{eoL})Q_{\text{bat}}} \quad , \quad (22)$$

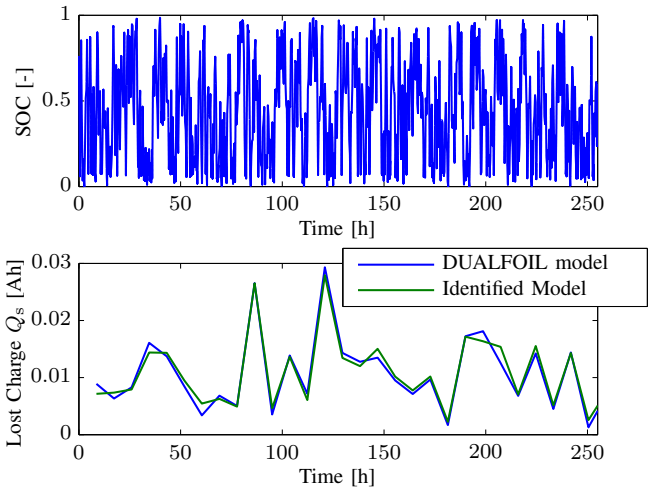

Figure 4. SOC variation (top) and lost charge (bottom) during the battery degradation ID process given an arbitrary stimuli pattern and Q_{bat} measurements every 6 approximately full cycles. The RMSE between the DUALFOIL model and the model prediction $\boldsymbol{M}\hat{\boldsymbol{I}}_s$ is 1.3e-3.

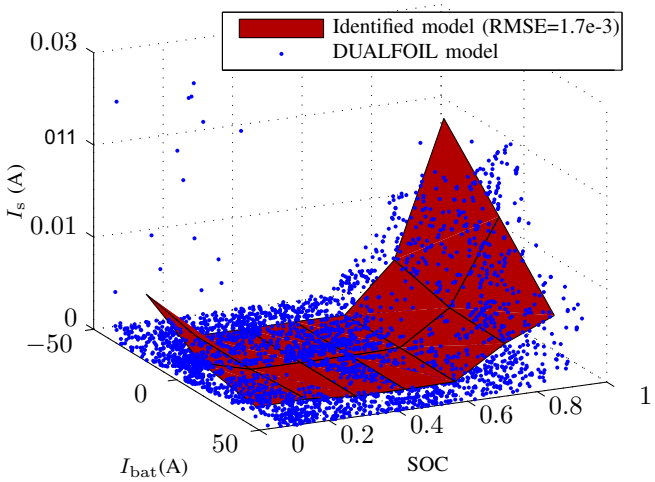

Figure 5. Identified degradation map (red) of estimated side current I_{s} as a function of the SOC and discharge/charge (pos/neg) applied battery current I_{bat} compared to degradation values obtained from the DUALFOIL model (blue).

resulting in a cost map, as shown in Fig. 6 (blue) for c_{inv} = 400€/(kWh). We aim to calculate the maximum possible profit and so we set eoL = 0. Since battery control inputs are usually given in the power domain, not the current domain, we also transform the current axis into a power axis (normalized by the battery capacity), as shown in the figure. The cost map can be approximated with a positive semi-definite quadratic cost function

$$J_{\text{bat}} = b(SOC - a)^2 + cu_{\text{gen}}^{\text{bat}} + du_{\text{load}}^{\text{bat}} + eu_{\text{load}}^{\text{bat}\,2} \quad , \quad (23)$$

which is compliant with a quadratic MPC framework. The parameters a, b, c, d, e listed in Table IV were determined by a LS fit minimizing the distance between the cost map and the cost function shown in Fig. 6.

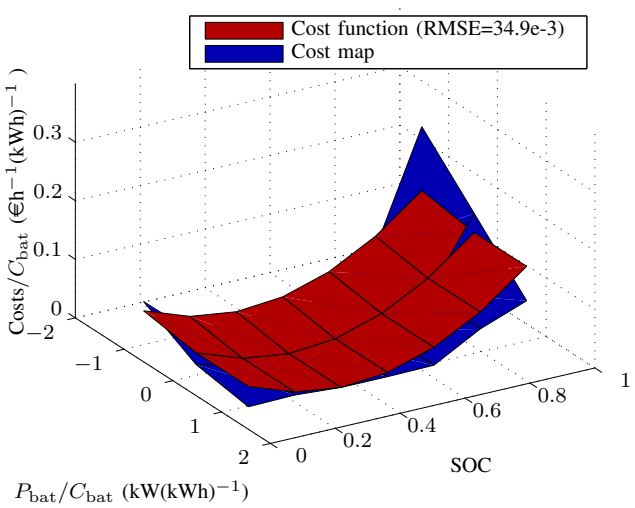

Figure 6. Degradation cost map and approximate quadratic cost function.

Table IV
IDENTIFIED DEGRADATION COST PARAMETERS

a	0.37		SOC target
b	0.42	€C_{bat} h^{-1}(kWh)$^{-1}$	cost parameter SOC
c	0	€(kWh)$^{-1}$	cost parameter u_{gen}
d	6.5e-3	€(kWh)$^{-1}$	cost parameter u_{load}
e	6e-3	€kWh (kW)$^{-2}$ h^{-1} $C_{\text{bat}}{}^{-1}$	cost parameter u_{load}^2

IV. Case Study: Peak Shave Application

We now show how the degradation cost function and battery model can be used within an MPC framework to achieve peak shaving, and then we compare the results to those of a heuristic control approach. In each case, we assume an industrial customer is charged for power and energy utilization, and uses a battery to both reduce its power peak demand $u_{\text{gen,max}}^{\text{net}}$ and exploit price differences in energy prices.

A. MPC Design

We use the Power Nodes Framework [11] to formulate the MPC problem as a Quadratic Programming (QP) problem. We try to find the optimal trajectory $\boldsymbol{U}$ that minimizes following optimization problem

$$\min_{\boldsymbol{U}\in\boldsymbol{u}^N} T_{\text{s}} \sum_{k=1}^{N} J_{\text{bat}}(k) + c_{\text{net}}(k) u_{\text{gen}}^{\text{net}}(k) \quad , \quad (24)$$

s.t. (13) ,

$$SOC_{\text{L}} \leq x_1(k) + x_2(k) \leq SOC_{\text{H}} \quad , \quad (25)$$

$$x_1(k) \leq c_{\text{w}} \quad , \quad (26)$$

$$x_2(k) \leq 1 - c_{\text{w}} \quad , \quad (27)$$

$$u_{\text{gen}}^{\text{bat}}(k) + u_{\text{gen}}^{\text{net}}(k) - u_{\text{load}}^{\text{bat}}(k) - P_{\text{load}}^{\text{G2}}(k) = 0 \ , \quad (28)$$

$$u_{\text{gen}}^{\text{net}}(k) \leq u_{\text{gen,max}}^{\text{net}} \quad , \quad (29)$$

$$u_{\text{load}}^{\text{bat}}(k) \leq P_{\text{bat,r}} \quad , \quad (30)$$

$$u_{\text{gen}}^{\text{bat}}(k) \leq P_{\text{bat,r}} \quad , \quad (31)$$

where k is the time step, $\boldsymbol{u} = [u^{\text{bat}}_{\text{load}}, u^{\text{bat}}_{\text{gen}}]^T$, $P^{\text{G2}}_{\text{load}}$ is the fixed consumption profile of the industrial customer, and $u^{\text{net}}_{\text{gen}}$ is the net grid injection, defined as in (28). Equation (24) is the MPC objective, which includes the battery cost function and net grid injection costs. Equation (13) is the linear extended battery model in discrete time. Equation (25) bounds the SOC and (26)-(27) prevent an overflow of the wells (x_1, x_2). Equation (29) ensures that $u^{\text{net}}_{\text{gen}}$ does not exceed a threshold $u^{\text{net}}_{\text{gen,max}}$, which we assume is chosen a priori, and (30)-(31) specify the power bounds of the battery.

We apply our control actions to the DUALFOIL model used in place of a real battery system. To correct for model mismatch, we use receding horizon control, resolving the optimization problem with new state information from a Luenberger observer that uses the true SOC value from the DUALFOIL model every R_{t} hours using a time horizon of H_{t} hours.

B. Heuristic Control Design

Algorithm 1 lists heuristic control actions for peak shaving, assuming a two-part electricity tariff with prices T_{lo} and T_{hi}. If $P^{\text{G2}}_{\text{load}}$ is higher than the peak threshold $u^{\text{net}}_{\text{gen,max}}$ (step: 2), then the battery is discharged. Otherwise, the battery is charged to a fixed SOC level, either SOC_{H} or SOC_{L} depending upon the current electricity price (step: 8-9).

Algorithm 1 Heuristic controller for a peak shaving.

1: **for** $(k = 1 : L)$ **do**
2: **if** $(P^{\text{G2}}_{\text{load}}(k) \geq u^{\text{net}}_{\text{gen,max}})$ **then**
3: $u^{\text{bat}}_{\text{gen}}(k) = P^{\text{G2}}_{\text{load}}(k) - u^{\text{net}}_{\text{gen,max}}$
4: **if** $(u^{\text{bat}}_{\text{gen}}(k) > P_{\text{bat,r}})$ **then**
5: $u^{\text{bat}}_{\text{gen}}(k) = P_{\text{bat,r}}$
6: **end if**
7: **else**
8: **if** $((SOC(k) < SOC_{\text{H}} \&\& T_{\text{lo}})$
9: **or** $(SOC(k) < SOC_{\text{L}} \&\& T_{\text{hi}}))$ **then**
10: $u^{\text{bat}}_{\text{load}}(k) = u^{\text{net}}_{\text{gen,max}} - P^{\text{G2}}_{\text{load}}(k)$
11: **if** $(u^{\text{bat}}_{\text{load}}(k) > P_{\text{bat,r}})$ **then**
12: $u^{\text{bat}}_{\text{load}}(k) = P_{\text{bat,r}}$
13: **end if**
14: **end if**
15: **end if**
16: **end for**

C. Simulation & Results

We use the parameters and assumptions listed in Table V. We test three controllers: 1) the heuristic controller, 2) the MPC controller without degradation costs ('MPC standard'), and 3) the MPC controller with degradation costs ('MPC degrad'). We apply each controller to the same system for a one month period, acquire the capacity fade from the DUALFOIL model, and extrapolate the results to determine the battery lifetime at a specific eoL criterion. Figure 7 shows sample simulation results from 'MPC degrad.' Fig. 8 shows the SOC resulting from different controllers.

An important quantity that allows us to assess the economic viability of an investment is the IRR. To calculate the IRR,

Table V
SIMULATION PARAMETERS AND ASSUMPTIONS

n_{cell}	106	number of DUALFOIL cells in series
A_{cell}	7.9 m^2	cell area
$\bar{V}_{\text{oc}}$	400 V	average open circuit potential
C_{bat}	100kWh	energy capacity
$P_{\text{bat,r}}$	30kW	battery power
$u^{\max}_{\text{gen,net}}$	80kW	peak shave threshold
$P^{\text{G2}}_{\text{load}}$	100kWp	G2 standard industrial load profile [14] from Jan 2012 (monthly consumption 18.6MWh)
c_{net}	EWZ NNB power price	industrial net tariff of Zurich utility (EWZ) 9€/kW per month
	energy price	60€/MWh (day), 30€/MWh (night)
T_{s}	15min	sample rate
H_{t}	24h	time horizon
R_{t}	12h	receding horizon window

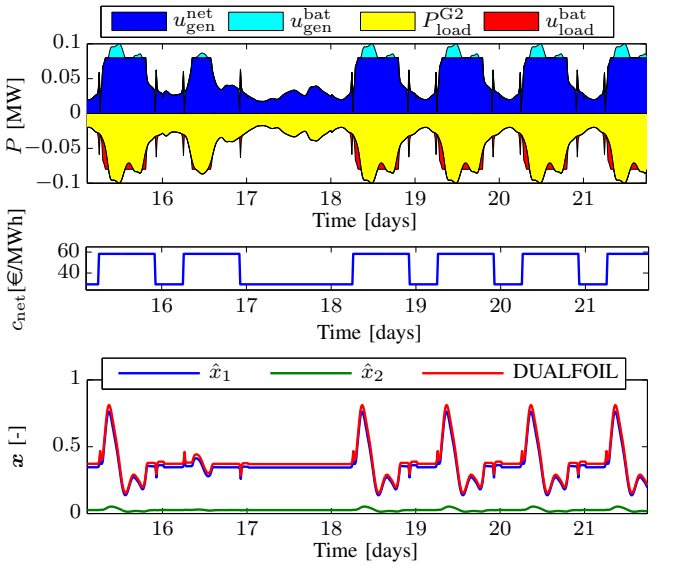

Figure 7. Simulation results from the MPC approach including the quadratic degradation cost function.

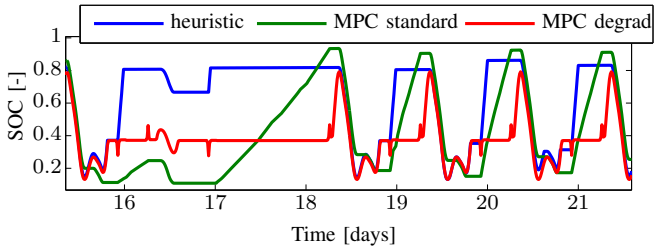

Figure 8. Comparison of the SOC resulting from the different controllers.

we solve

$$-C_{\text{bat}} c_{\text{inv}} + \sum_{n=1}^{L} \frac{c_{\text{EP}} - c^{\text{bat}}_{\text{EP}}}{(1+\text{IRR})^n} = 0 \qquad (32)$$

for the IRR, where $c_{\text{EP}} - c^{\text{bat}}_{\text{EP}}$ is the energy and power utilization costs saved with a battery investment and L is the battery lifetime in years.

The controller configurations, the IRRs, and battery lifetimes L results are summarized in Table VI. Instead of explicitly accounting for degradation costs, the 'MPC standard'

Table VI
COMPARISON OF PROPOSED CONTROLLERS @ EOL = 0.5

Controller	heuristic	MPC standard	MPC degrad
Parameters	$SOC_{\mathrm{H}} = 0.8$ $SOC_{\mathrm{L}} = 0.3$	$SOC_{\mathrm{H}} = 0.78$ $SOC_{\mathrm{L}} = 0.1$ a = 0 b = 0€/h c = 0€/(MWh) d = 0€/(MWh) e = 0€/((MW)^2 h)	$SOC_{\mathrm{H}} = 1$ $SOC_{\mathrm{L}} = 0$ a = 0.37 b = 42€/h c = 0€/(MWh) d = 6.5€/(MWh) e = 60€/((MW)^2 h)
Battery lifetime (L)	13 months	7.3 years	19 years
Internal Rate of Return (IRR)	-69%	-8%	3.1%
Achievable full cycles	206	1672	4651

controller uses a reduced SOC range to heuristically avoid degradation. We tuned the bounds of the SOC range to achieve the best battery lifetime. Despite the tuning, the 'MPC degrad' approach performs much better, increasing the battery lifetime and resulting in a positive IRR.

Note that we also attempted to use the linear basic battery model within our MPC algorithm and found that for this application, the results were identical to those generated with the extended basic battery model. This is because, for this application, the battery is not driven to extreme high or low SOCs.

V. CONCLUSION AND OUTLOOK

In this paper, we presented methods to model and identify fast battery dynamics and slow battery degradation processes. Though we have assumed Li-ion batteries within this paper, our methods could be applied to different chemical storage technologies such as NaS, or lead acid. These models allow us to optimally control batteries for power system applications. We presented four different models that capture fast battery dynamics, and showed how one can identify the parameters of the nonlinear models and use them to compute the parameters of the linear models. The models were identified and validated on the high-fidelity Li-ion DUALFOIL model. We use a linear extended battery model within our controller. This model is able to capture the rate capacity effect, which allows us to accurately model the capabilities of the battery in high/low SOC regimes.

We also developed a method to identify battery degradation. The method can be used on battery systems stimulated with arbitrary patterns that could correspond to those in real battery applications. Thus, this method could be run online. The result is a degradation map that describes the impact of discrete types of control actions on the lost battery charge. The degradation map is transformed to an economic cost map from which a quadratic cost function is derived. This economic cost function can be incorporated into a quadratic MPC framework that relies on an economic objective function. Thus, the objective function operates solely within the cost domain, avoiding the need for a multi-objective formulation. Finally, we have shown through simulation that the MPC approach is able to extend battery lifetimes and increase IRRs as compared to conventional control approaches.

There are many avenues for future research. The degradation process represented within the DUALFOIL model may not correspond to that of a real battery, and so it will be important to investigate the performance of the approaches on real systems. Using the DUALFOIL model has given us valuable insight into degradation modeling and a preliminary validation of our methodology; however, the quantitative values presented in this paper (battery lifetimes, IRRs, etc.) should be understood in relative, not absolute, terms. Important questions for the future include whether the stationary degradation process serves a good approximation of the real process and how sensitive the economic results are to the battery model and parameters.

ACKNOWLEDGMENT

The authors would like to thank the Swiss Commission for Technology and Innovation (project no. 14478).

REFERENCES

[1] S. Schoenung, "Energy storage systems cost update," Sandia National Laboratories, Tech. Rep. SAND2011-2730, 2011.

[2] P. Poonpun and W. Jewell, "Analysis of the cost per kilowatt hour to store electricity," *Energy Conversion, IEEE Transactions on*, vol. 23, no. 2, pp. 529–534, 2008.

[3] S. Moura, J. Stein, and H. Fathy, "Battery-health conscious power management in plug-in hybrid electric vehicles via electrochemical modeling and stochastic control," *Control Systems Technology, IEEE Transactions on*, vol. 21, no. 3, pp. 679–694, May 2013.

[4] M. Koller, T. Borsche, A. Ulbig, and G. Andersson, "Defining a degradation cost function for optimal control of a battery energy storage system," in *PowerTech (POWERTECH), 2013 IEEE Grenoble*, 2013, pp. 1–6.

[5] T. F. Fuller, M. Doyle, and J. Newman, "Simulation and optimization of the dual lithium ion insertion cell," *Journal of The Electrochemical Society*, vol. 141, no. 1, pp. 1–10, 1994.

[6] M. Doyle and J. Newman, "Analysis of capacity-rate data for lithium batteries using simplified models of the discharge process," *Journal of Applied Electrochemistry*, vol. 27, no. 7, pp. 846–856, 1997.

[7] E. Vrettos and S. Papathanassiou, "Operating policy and optimal sizing of a high penetration RES-BESS system for small isolated grids," *Energy Conversion, IEEE Transactions on*, vol. 26, no. 3, pp. 744–756, 2011.

[8] A. Di Giorgio, L. Pimpinella, and F. Liberati, "A model predictive control approach to the load shifting problem in a household equipped with an energy storage unit," in *Control Automation (MED), 2012 20th Mediterranean Conference on*, 2012, pp. 1491–1498.

[9] O. Tremblay, L.-A. Dessaint, and A.-I. Dekkiche, "A generic battery model for the dynamic simulation of hybrid electric vehicles," in *Vehicle Power and Propulsion Conference, 2007. VPPC 2007. IEEE*, sept. 2007, pp. 284 –289.

[10] J. F. Manwell and J. G. McGowan, "Lead acid battery storage model for hybrid energy systems," *Solar Energy*, vol. 50, no. 5, pp. 399 – 405, 1993.

[11] K. Heussen, S. Koch, A. Ulbig, and G. Andersson, "Energy storage in power system operation: The power nodes modeling framework," in *Innovative Smart Grid Technologies Conference Europe (ISGT Europe), 2010 IEEE PES*, Oct. 2010.

[12] P. Ramadass, B. Haran, P. M. Gomadam, R. White, and B. N. Popov, "Development of first principles capacity fade model for Li-ion cells," *Journal of The Electrochemical Society*, vol. 151, no. 2, pp. A196–A203, 2004.

[13] G. L. Plett, "Recursive approximate weighted total least squares estimation of battery cell total capacity," *Journal of Power Sources*, vol. 196, no. 4, pp. 2319 – 2331, 2011.

[14] Bayernwerk. [Online]. Available: https://www.bayernwerk.de/pages/eby_de/Netz/Stromnetz/Netzzugang/Lastprofilverfahren/Standard_Lastprofile/index.htm